# Shape-Locking Mechanism of Flexible Joint Using Mechanical Latch With Electromagnetic Force

Deok Gyoon Chung, Joonhwan Kim, DongHoon Baek, Joonyeong Kim, and Dong-Soo Kwon

***Abstract*—Single-incision laparoscopic surgery (SILS) has emerged as a procedure to further improve cosmetic profits and reduce the postoperative pain of multiport laparoscopic surgery. However, SILS is a difficult operation due to the limited workspace or accessibility. To improve surgical convenience, flexible surgical robots should be developed and applied to SILS for a large workspace. Flexible robots would penetrate a single incision point around the navel area and can provide a large workspace within the abdominal cavity. However, it is difficult to support the force required for surgical intervention during this process. In this study, a novel mechanism to lock the shape of a flexible joint to support the external forces during SILS is proposed. The developed shape-locking mechanism involves placing a latch between the joints; the shape locks by engagement of the latches via an electromagnetic force. The mechanism is implemented through mechanical coupling, so it can withstand large loads. Furthermore, the driving force of the mechanism is small because it only needs to engage the latch structure. This letter discusses the development of the mechanism, magnetic force simulation, and a payload experiment.**

***Index Terms*—Surgical Robotics, Laparoscopy, Flexible Robots, Mechanism Design.**

## I. Introduction

SINGLE-INCISION laparoscopic surgery (SILS), which is performed through only one invasion point, is regarded as the next advancement of surgical procedures [1]. In this procedure, an incision with a diameter of 30 mm is made in the navel area, and a surgical instrument and an endoscope are inserted through the incision to perform the operation. SILS minimizes recovery time and does not leave a visible scar on patients [2].

A variety of rigid-type robot systems for SILS have been developed [3]–[8]. However, rigid-type robots have a limited working area within the abdominal cavity. Thus, the operations that can be performed by this type of robot are limited. If SILS is performed by a flexible robot (Fig. 1), this problem can be solved by providing a wider working area in the abdominal cavity. However, when performing medical interventions, such as tissue resection, perforation, biopsy, and suturing, surgical robots must maintain strength and firmness to improve the stability of the operation [9]. In short, the robot should be flexible enough to approach the affected area, but rigid enough to provide an operational stability. The shape-locking mechanism may be a solution to this tradeoff problem [10].

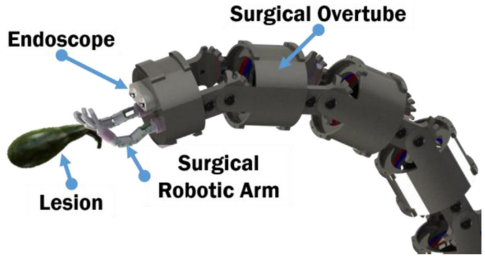


Fig. 1. Conceptual design of the flexible SILS robot.

Various research groups have studied shape-locking mechanisms for flexible surgical robots. Recent studies have suggested methods that use friction, a phase change of the material, and a mechanical locking.

USGI Medical Inc.'s TransPort has a ring on the outer part of the flexible joint, and the pulling of a cable fixes the shape using the friction between the rings [11]. Kim *et al.* altered the stiffness by forming multiple layers of polymer material and creating a vacuum the periphery, thereby increasing the inter-layer friction [12]. The granular jamming principle, in which the stiffness is changed by changing the pressure difference of a membrane, is also used. Granular jamming is applied to endoscopic applications with an overtube for colonoscopies [13]. Zuo proposed a mechanism to lock the shape using a flexible serrated link, a bellows tube, and air pressure. By adjusting the air pressure inside the tube, the frictional force between the serrated links maintains the shape [14].

The above-mentioned methods are based on frictional force. Friction-based locking constrains motion by using the friction between two parts. In order to increase the force that locks the shape, a larger frictional force is required, and a larger driving force is required to drive the mechanism. Furthermore, a mechanism requiring a large driving force must have a large diameter or a complicated structure [19]. Therefore, in the case

Manuscript received September 10, 2018; accepted January 4, 2019. Date of publication February 1, 2019; date of current version May 8, 2019. This letter was recommended for publication by Associate Editor E. Rouse and Editor P. Valdastri upon evaluation of the reviewers' comments. This work was supported in part by NRF National Research Foundation of Korea Grant funded by the Korean Government (NRF-2017-Fostering Core Leaders of the Future Basic Science Program/Global Ph.D. Fellowship Program) and in part by the Korea Health Technology R&D Project through the Korea Health Industry Development Institute (KHIDI), funded by the Ministry of Health & Welfare, Republic of Korea under Grant HI17C2012. *(Corresponding author: Dong-Soo Kwon.)*

D. G. Chung, Joonhwan Kim, Joonyeong Kim, and D.-S. Kwon are with the Division of Mechanical Engineering School of Mechanical, Aerospace and Systems Engineering, Korea Advanced Institute of Science and Technology, Daejeon 34141, South Korea (e-mail: jdk0403@kaist.ac.kr; te108715@gmail.com; kimjy091@kaist.ac.kr; kwonds@kaist.ac.kr).

D. Baek is with the Robotics Program, Korea Advanced Institute of Science and Technology, Daejeon 34141, South Korea (e-mail: romansabaek@kaist.ac.kr).

Digital Object Identifier 10.1109/LRA.2019.2897006

of a flexible surgical robot, which has diameter restrictions, a friction-based shape-locking mechanism limits the stiffness.

Other research groups have devised shape-locking mechanisms using the phase change of a shape memory alloy (SMA) with a relatively low melting point [15]–[16]. If flexibility is required, the temperature of the SMA can be increased to transform it into a liquid state, and when rigidity is needed the temperature is decreased. However, this mechanism takes several seconds to change between the phases. Further technical advances are necessary to apply the SMA phase change method in surgical situations, particularly those that require rapid responses in an emergency.

Some research groups have suggested a shape locking mechanism using the mechanical locking driven by electromagnetic force. Some applications of this include a coupling mechanism of a modular robot [17] and a robot hand-locking mechanism to increase the lifting force [18]. This method has the advantage that it can withstand more force than other methods, and has a simple structure with fast reaction speed. This locking mechanism has been widely used in robotics. In this study, a novel shape-locking serial joint based on electromagnetic driven latch coupling mechanism is presented. Its unique features of simplicity, compactness, low driving force, and fast reaction time make the proposed flexible joint suitable for an application to surgical overtube for SILS.

For mechanical locking, the strength of the material determines the lock, which is generally much stronger than friction-based locking. In addition, it requires only the force to move the mechanical component to the locking position, thus consuming low amounts of energy [19]. A disadvantage of mechanical locking is the limited number of locking positions. Therefore, an extended latch structure is devised, which locks the shape at various angles.

When an electromagnetic force is used, the driving mechanism is simplified because it consists of only two wires at the end of the surgical overtube. Moreover, a bidirectional force could be realized without an additional mechanism by changing the direction of the current, thus simplifying the mechanism. In addition, the reaction rate is faster than other force transfer methods because there is no continuous force transfer medium.

The following section explains the principle and design of the proposed shape-locking mechanism, and in Section III the simulation and verification of the mechanism is described. In Section IV, we discuss about proposed mechanism comprehensive discussion. Then conclusions and further required research are described.

## II. Method

An overtube with the proposed shape-locking mechanism is developed as shown in Fig. 2. This overtube is able to hold the shape strongly at various curvatures. Surgical instruments and endoscopes are equipped through its internal channel.

### A. Principle of Shape Locking

As shown in Fig. 3, the joints are integrated with the hooks, and the magnets is integrated with the pawls. Three components

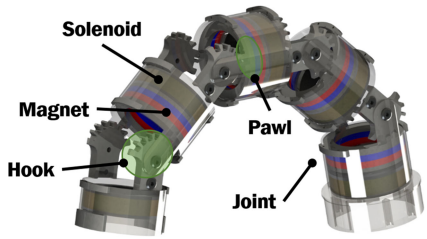


Fig. 2. Representation of the shape-locking mechanism of the flexible joint using mechanical latches and magnetic force.

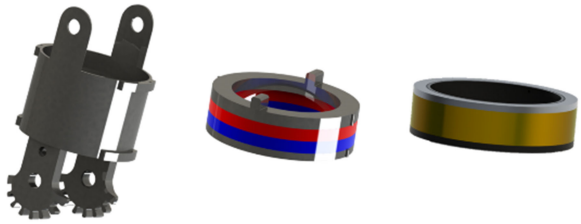

Fig. 3. Mechanism components: joint and hook (left), magnet and pawl (center), solenoid (right).

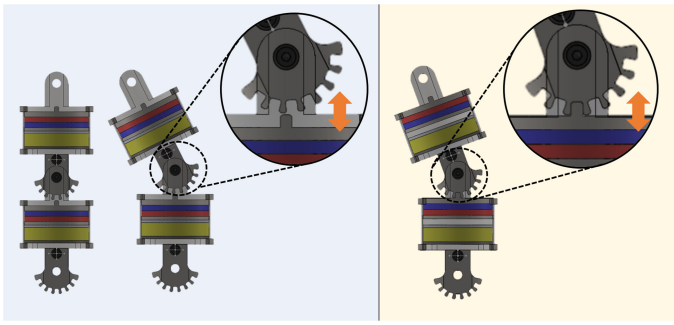

Fig. 4. Operation principle, locking-off (left), locking-on (right).

are placed on each joint. A solenoid is placed in the joint. A hook is placed between the joints, and the pawl is moved inside the joint to drive the locking mechanism. The pawl is attached to a magnet and could move by the magnetic force.

When the flexible joint is moved into the operative position, the force induced by the steel core of the solenoid acted upon the magnet. At that time, the magnet and the solenoid is attached and do not affect the rotation of the flexible joint (left image, Fig. 4). To lock the joint, a current is sent through the solenoid to form the same magnetic pole as the magnet. The solenoid pushed the magnet, and the pawl engaged with the hook (right image, Fig. 4). In this case, the joint shape remains firm even if an external force was applied. To unlock the joint, a current is applied in the opposite direction, releasing the latch and ensuring flexibility.

### B. A Single Joint With Shape-locking Mechanism

*1) Design Specification:* The developed overtube is devised to meet the following design goals. First, the total external diameter is set to 28 mm, which is appropriate for avoiding scarring when SILS is performed [2]. It has been reported that when the

robot enters through the navel, the maximum outer diameter of the orifice is 30 to 35 mm [2], [8]. A hollow neodymium magnet is used inside the joint with an outer diameter of 25 mm, and the inner diameters of both the magnet and overtube are 20 mm. The pawls between the joints are in pairs, with a total of seven grooves per joint at 20° intervals (Fig. 4), so each joint can be locked at intervals of 20.

*2) Mechanical Modeling of Deflection:* In this section, the stiffness of the shape-locked state in a single joint of the overtube is theoretically obtained and compared with the simulation. This analytical solution will then determine the dimensions of the latch structure.

In SILS, the force requirements are based on supporting the liver, which is the heaviest organ in the human body. The liver has an average weight of approximately 15 N [18]. This value is used as the baseline value for the greatest amount of force that surgical instruments undergo. The proposed locking mechanism aims to provide stable support when applying a force of up to 20 N considering the safety factor. In this study, the aim of the latch element is to have almost no theoretical deflection, which is vulnerable to fracture at the single joint mechanism. In the proposed shape locking, the determinant of rigidity is not the slip or detachment of the material but the deflection of the structure, especially the deflection of the latch. The deflection amount of the single joint mechanism is set to about 0.05 mm as a target value which can be regarded as almost no deflection with respect to the load. According to this target value, the dimensions of the latch were determined through deflection analysis and FEM simulation.

The theoretical stiffness of a single joint is obtained by using the moment-area method, which is a method of solid mechanical analysis. The moment area method is used to obtain the deflection of a structure, having segments with various area moments of inertia I, with a simple calculation when a force is applied [21]. The stiffness and deflection are calculated by the moment-area method as follows. First, the bending moment diagram (BMD) is plotted, then divided into sections by the moment of inertia. Each cross section area on the BMD is multiplied by the distance from the centroid of the moment area to a 'target point', at which the final deflection is determined. Then, the result is divided by the section's moment, and the elastic modulus leads to deflection of the target point.

$$\delta = \frac{\bar{x} A_m}{EI} \tag{1}$$

The basic formula is as above. The deflection of the target point is represented by $\delta$, the distance from the centroid of the moment area to the target point in each section on the BMD is given by $\bar{x}$, and the each cross section area on the BMD is expressed as $A_m$.

A single joint is divided into 5 sections, as shown in Fig. 5. In particular, the fourth section portrays the pawl and hook of the latch; most of the deflection occurred at this section. With the assumption that the force is concentrated at the distal end of the joint, this point is set as the target point and the deflection is obtained. The bending moment is proportional to the distance from the target point (Fig. 6). The modified formulas for each section are as follows.

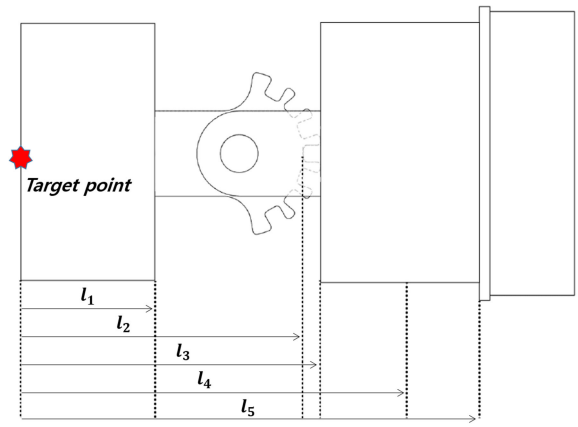


Fig. 5. Sections of a single joint.

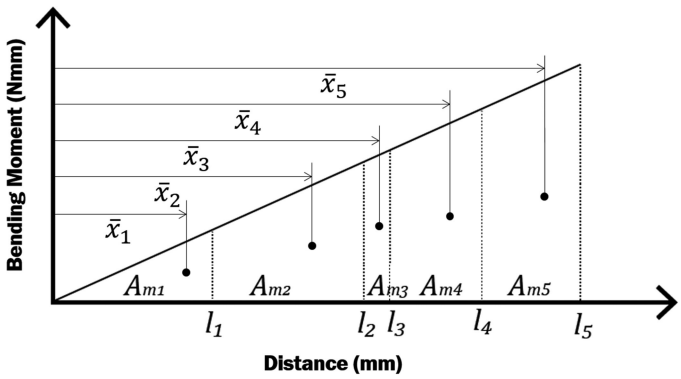


Fig. 6. Bending moment diagram of a single joint.

$$\delta_{tot} = \delta_1 + \delta_2 + \delta_3 + \delta_4 + \delta_5 \tag{2}$$

$$\delta_i = \frac{\bar{x}_i A_{mi}}{E_i I_i}, \ (i = 1, 2, 3, 4, 5) \tag{3}$$

From the calculation results, most deflection occur in the latch $(A_{m3})$. Each groove should have a width of 1.8 mm, a height of 2 mm, and a thickness of 3 mm so that the total deflection is 0.050 mm. All mechanical parts, except the magnets, were machined from SUS 304 material. The deflection that occurs in this case meets the reference objective. Detailed calculation information is attached with the appendix.

The results of the FEM simulation (SolidWorks simulation 2016, DASSAULT SYSTÈMES, France) shows a deflection of 0.06 mm, with no significant difference to the analytical solution (Fig. 7). The validity of the theoretical calculation results is proved by matching the FEM simulation.

*3) Magnetic Force Analysis:* From the electromagnetic FEM simulation (Ansys Maxwell 16.02, ANSYS Inc, USA), the amount of current required to drive the mechanism is derived.

Firstly, the dimensions of the solenoid are selected by considering the internal size of the joint; the solenoid has a winding of 0.07 mm with 1200 turns. The magnetomotive force, F could

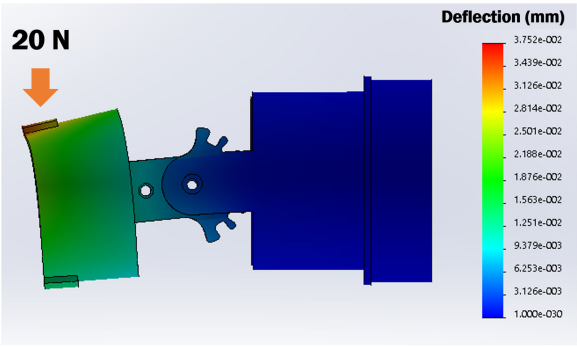


Fig. 7. Simulation results of a single overtube joint.

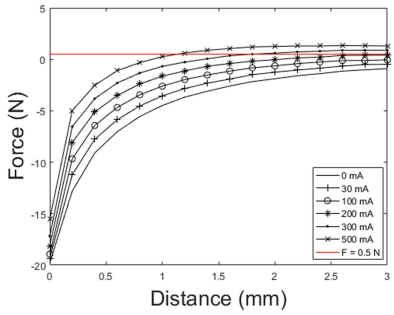


Fig. 8. The repulsive force versus distance between the magnet and solenoid for various current values.

be calculated according to the diameter of the conductor

$$F = NI \ [A \cdot turns, \ AT] \tag{4}$$

Where N is a total number of windings which can be expressed as,

$$N = N_w N_h = \frac{w}{d_c} \cdot \frac{h}{d_c} \tag{5}$$

where, I is a current [A], w is a width and height of the solenoid [mm], and $d_c$ is a diameter of the coated wire [mm].

The current is selected to lift the weight of the magnet and latch in consideration of friction. Therefore, the load is set to 0.5 N or more (total weight of the magnet and latch: 0.1 N). As a result of various simulations with varying current and distance between the magnet and solenoid, it is confirmed that 300 mA could generate the required force (Fig. 8). Simultaneously, a magnetomotive force of 360 A T is generated by winding the conductor 1200 times; these specs are applied to the simulation. Fig. 8 shows the repulsive force the magnet received from the solenoid in the single joint state. It is found that the solenoid and the magnet must be separated by at least 2.8 mm in order to receive a positive repulsive force, raising the magnet when the solenoid is operating (360 A T) and producing a negative force by the steel core when not operating (0 A T).

### C. Development of a Continuum Joint

*1) Implementation:* An overtube consisting of four joints was fabricated as the testbed. The overall length of the overtube was 121.6 mm, and the length per joint was 36.5 mm. The resolution of the locking mechanism of each joint in the overtube is 20°. Since each joint has seven grooves, total of 343 locking posture is possible. The maximum possible locking angle is 180° when each joint is at 60° to its neighbor.

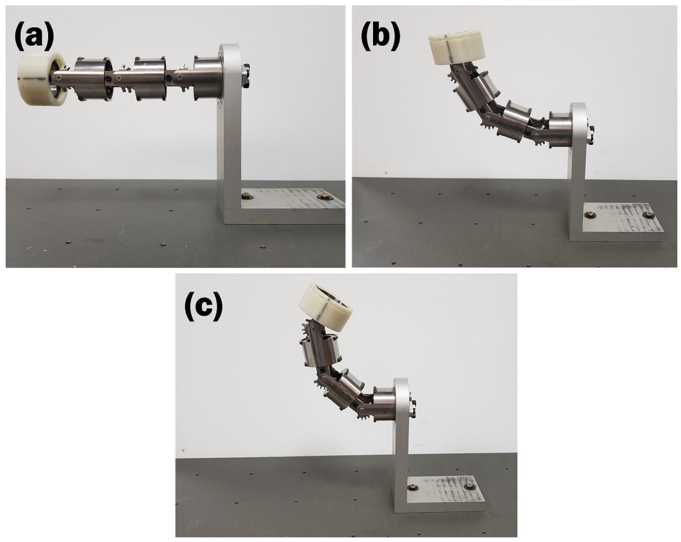


Fig. 9. Various postures of overtube: (a) straight posture, (b) tip orientation of 60°, (c) tip orientation of 120°.

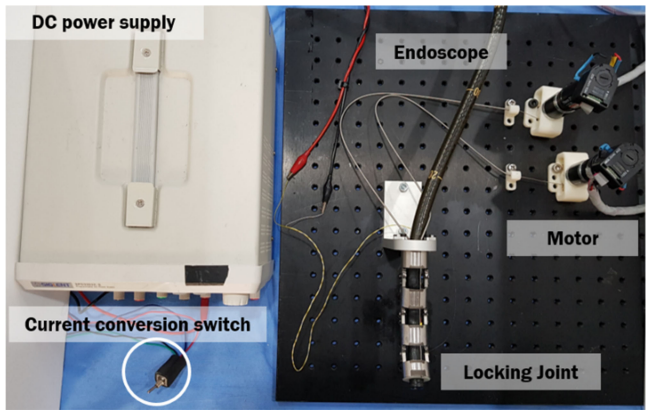


Fig. 10. Actuation and transmission system.

Fig. 9 shows various joint postures. The developed overtube had two degrees of freedom (DOFs) composed of one bending and one rotation. As shown in Fig. 9(a), it deformed from a straight posture to a bending posture as in Figs. 9(b) and (c). A current was applied to the solenoid when the surgical overtube required shape-locking. Then, the latches between the joints were engaged to lock the overtube shape. When the shape was locked, it was firmly fixed against external forces.

*2) Actuation and Transmission System:* The bending DOF of the joint was driven through the actuation cable. The system that controlled the overtube comprised of a motor control unit that controlled the joint bending angle, and a current control unit that drove the latch by applying a current, as shown in Fig. 10.

The actuation cable was tied at one end of the overtube, passed through every joint, and was tied to the motor at the opposite end. This method was relatively simple and required a small

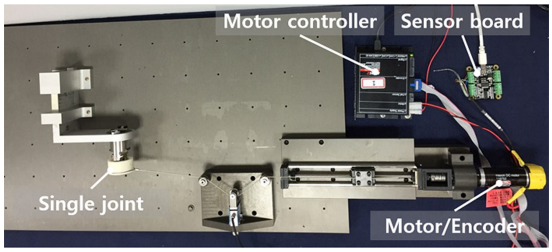


Fig. 11. Experimental testbed for single joint mechanism.

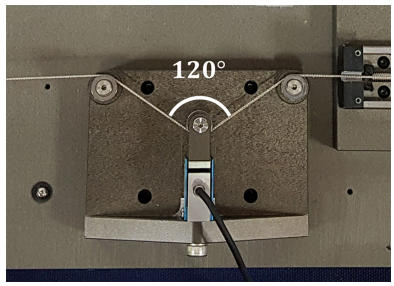


Fig. 12. Tension-measuring module.

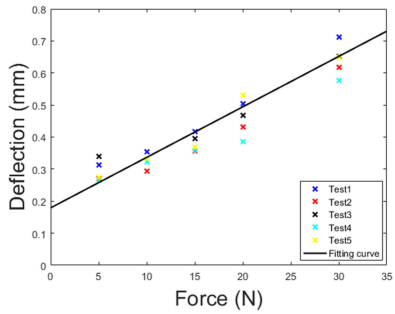


Fig. 13. Experimental results of the single joint mechanism.

number of components. A SUS cable with a diameter of 1 mm was used. The cable was attached on both sides of the overtube to control the clockwise and counterclockwise bending.

Two actuators were used to drive the overtube. The pulleys were fixed to the actuators, and the cable were fixed to the pulleys to drive the overtube. Two 10 W DC motors, both with 19:1 gear ratios, were used (DC 118752, maxon motor). The maximum continuous torque of the motor was 532 mN·m, and the maximum output was 53.2 N when considering the gear head and pulley. The diameters of the pulleys were 20 mm and all were fixed to a table.

A typical AC-to-DC converter (SPD3303X-E, SIGLENT Technologies) was used to supply the current. Up to 64 V could be applied to the solenoid. For proposed shape locking mechanism, the electric power used for each solenoid is 9.6 W (300 mA and 32 V each). The current direction could easily be changed using the current conversion switch, which allows instant on/off switching of the locking mechanism.

## III. Verification Through Simulation and Experimentation

### A. Stiffness of Locking Mechanism

In this section, the analysis of the mechanism and the stiffness measurement experiment are described. To verify the theoretical results, we measured the deflection and stiffness of the fabricated mechanism through experimentation. An experimental testbed was constructed for this purpose, an overview of which is shown in Fig. 11. The testbed consisted of a DC motor to drive the actuation cable and a tension-measuring module. The overtube was fixed to the surface plate, and a motor was used to apply a force to the joint by pulling the cable. The force applied to the overtube was then measured using the tension-measuring module and the motor encoder measured the deflection.

The ball screw was connected to the motor and pulled the overtube linearly. The pitch of the ball screw was 1 mm, which was suitable for the measurement of microdisplacement. The tension was measured by a load cell (333FDX, KTOYO) using the strain in the wire path. Fig. 12 shows the tension-measuring module and the path of the wire. The tension applied to the load cell was the sum of the vertical components of both tensions. The angle of the wire passing through the tension-measuring module was designed to be 120°. The force measured in the load cell was as follows.

$$F_{loadcell} = 2\,T\,\cos 60^\circ = T \tag{6}$$

According to equation 6, the force measured by the load cell was equal to the cable tension. The cable used in the experiment was made of a SUS material with a diameter of 1 mm. For the accuracy of the experiment, calibration was performed in advance to measure the self-elongation of the cable with respect to the load. The elongation of the cable was measured consistently and was removed from the experimental result of the total deflection. The experiment was repeated 5 times for each load (1, 5, 10, 15, 20, and 30 N). The experimental results are shown in Fig 13.

In the case of a single joint, a total deflection of 0.48 mm occurred at a weight of 20 N. This actual result differed from the FEM simulation result. Theoretically, a displacement of 0.05 mm should occur when a load of 20 N is applied. This is mainly due to the backlash and clearance of machining error. In particular, the backlash was 0.19 mm, taken as the y-intercept value of the experimental result graph, and 0.26 mm extra strain occurred without backlash. Although it is a single joint mechanism, it consists of several machine parts. Therefore, when a joint receives a large force, there is a superposition of the deflection that overcomes the binding force of each part, which does not appear in the simulation. However, considering these factors, the deflection of 0.5 mm in the mechanism is superior to previous studies and is considered to be sufficient in practical use.

### B. Magnetic Force Interference in Continuum Joint

In this section, the scale of the effects of neighboring magnets on each other is derived. Fig. 14 shows the repulsive force that the magnets in the second joint received from the other solenoids in the multi-joint state. It can be seen that the magnet receives a positive repulsive force when the solenoid is operating (360

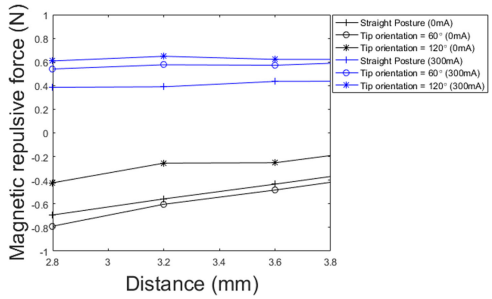


Fig. 14. Repulsive force versus distance between the magnet and solenoid at various bending angles in the multi-joint state.

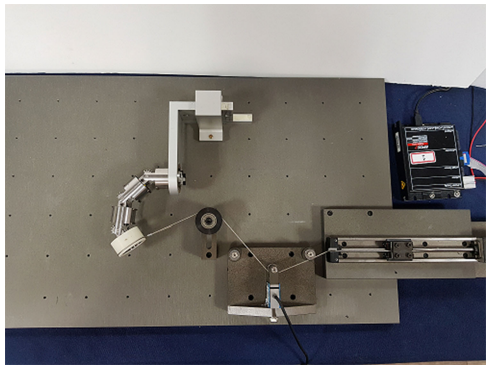

Fig. 15. Experimental testbed for the multi-joint mechanism.

A·T) and a negative force when not operating (0 A·T). This figure shows the larger the bending angle of a joint, the larger the magnetic field interference with the adjacent magnets when there is no electric current. However, it can also be seen that the magnet received a force of approximately 0.5 N when the current was applied, from the initial distance between the magnet and the solenoid (2.8 mm) to the final distance to which the latch is engaged (4.8 mm). The magnet–solenoid interference on the serial joint did not have a significant effect on driving.

### C. *Stiffness of Continuum Joint*

In this section, the experimental results of the proposed mechanism of multiple joints are derived and compared with existing shape-locking mechanisms. The overtube was developed with four joints (Fig. 9) and was fixed to the experimental testbed to measure the deflection and stiffness (Fig. 15). This experiment was conducted in the same way as that described in the previous experiment using single joint.

The overtube was tested for three different postures, as shown in Fig. 9. The experiment was repeated 5 times for each load (1, 5, 10, 15, 20, and 30 N). The load was applied perpendicular to the overtube.

Fig. 16 shows the experimental results for various postures of the overtube. With a straight posture and 4 serial joints, a total deflection of 2.6 mm occurred when the 20 N weight was applied. A total displacement of 2.2 mm occurred in the posture with a tip orientation of 60°, and a total displacement of 1.9 mm occurred in the posture of 120°. Because the torque acting length

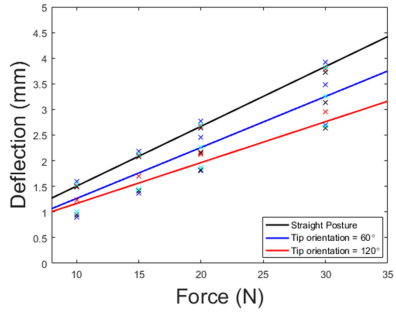


Fig. 16. Experimental results of the multi-joint mechanism: (a) straight posture, (b) tip orientation of 60°, (c) tip orientation of 120°.

changed at each posture, the results showed a difference.

$$\text{Flexural stiffness} = \frac{M}{k} \ \left(\text{Nmm}^2\right) \tag{7}$$

Where, $M$ is applied bending moment, and $k$ is curvature

Through the equation (7), the deflection value at the end can be converted into a stiffness unit expressed as $N$ mm$^2$ [22]. The stiffness of the proposed overtube with the straight posture is $1.38 \times 10^7 N$ mm$^2$.

The stiffness of the proposed shape-locking mechanism was higher than the others. According to the review article of shape-locking mechanism for medical device [10], proposed mechanism has about twice as much stiffness than layer jamming mechanism [12] which is regarded as having considerably high stiffness. Furthermore, the payload of the proposed mechanism is considerably larger than other flexible surgical robot studies. Because the proposed mechanism made use of a mechanical coupling method, there was a much greater stiffness than that in other methods.

## IV. Comprehensive Discussion

In this study, a shape-locking mechanism using a mechanical latch driven by an electromagnetic force was introduced, which can be applied to the surgical overtube of a flexible robot platform for SILS. The latch structure has the advantages that the force required to drive the mechanism is small while still being capable of withstanding a large load. These advantages have been demonstrated through stiffness measurement experiments. Furthermore, the electromagnetic FEM simulations have proven the drivability of the serial mechanism. However, the proposed mechanism has several considerations for clinical applications, as below.

When using mechanical locking, the number of locking positions is limited which may affect surgical performance. However, the role of the surgical overtube is to approach the lesion area and support the force during the surgical procedure. The internal robotic arm ensures the workspace and manipulability required for the operation. Therefore, the surgical overtube is sufficient for locking only in a limited number of postures because the internal flexible robot arm provides additional dexterity and workspace. It is also possible to cover additional workspace with outer tilting of the overtube in the locked state.

However, as there is currently no reference for this, an in-vivo experiment using the overtube to prove its usability will be conducted in the follow-up study.

A challenge with the latch-locking mechanism is the inability to engage/disengage the lock under a load. However, regarding usage of the overtube, this may not be necessary. When locking the mechanism, the bending–steering cable sustains the external forces, which does not apply to the latch structure. This is the same as locking off. When certain surgical procedures are completed and the robot is needed to be moved to other surgical sites, it is necessary to lock off the overtube. In this case, if a load is applied by the organ, the overtube can be moved to a position where the load can be removed through external motion and the locking mechanism can be released. However, in the case of an emergency, it is necessary to release the locking urgently. Therefore, the mechanism or control method for supporting the external force only by the joint steering cable during the locking off of the overtube will be studied further in future.

Regarding the characteristics of the mechanism when using an electric current, it is necessary to increase the safety. Firstly, the current value must be reduced to less than the safety current value (30 mA) and voltage (DC 60 V) [23]. This seems possible through the optimization process of the structure. Currently, the size of the moving magnet is considerably larger than the pawl of the latch. By reducing the volume and mass of this part, it is possible to drive even a small amount of current. If the volume and mass of the moving parts is reduced to 1/10 of the present design, the required force and the current is expected to decrease significantly. Secondly, the outside of the overtube will be wrapped with insulating rubber to prevent the current from flowing to the inside of the patient's body. Finally, the time of the current flow will be reduced. In present designs, the current must have a continuous flow in order to maintain the lock. When there is no current flow, the magnet receives the force attached to the iron core of the solenoid. There is a problem that the temperature increase of the solenoid and the steel core. Ideally, the locking/unlocking should be maintained even if no current is applied. This can be solved by placing the iron core on the opposite side of the solenoid. In the case of the mechanism in which the magnet and iron core are attached while there is no current flow, then when the current flows, the magnet becomes attached to the opposite iron core; the current will only be used for the purpose of a switch at the moment of locking on/off.

## V. Conclusion and Further Works

This letter presents the shape-locking flexible joint based on electromagnetic driven latch coupling mechanism. Experimental results demonstrated that shape locking mechanism worked well in a various curved configuration, and the rigidity at locked state is larger than the previous studies. In future research, an optimal structure of the proposed mechanism will be developed to improve the latch drivability and ensure the patient safety. In addition, we intend to modify the design to achieve 2-DOF bending, such as that used in endoscopy. Subsequently, various ex-vivo and in-vivo experiments will be conducted to determine the improvements for application in actual surgery. Finally, it is expected that the shape-locking mechanism using the latch structure may solve the limitations of conventional flexible surgical robots.

## Appendix

Variables (x-axis distance from BMD)

$l_1$ Length from the origin to the end point of each section on BMD

${l_1}^*$ Length of each section (length per section)

$c_i$ Length from the end of each section to the center of figure

$\bar{x}_i$ Length from the origin to each center of figure

$A_{mi}$ The area of each section

$I_i$ Area moment of inertia

$$\bar{x}_1 = l_1 - c_1,\ \ \bar{x}_2 = l_2 - c_2,\ \ \bar{x}_3 = l_3 - c_3,$$

$$\bar{x}_4 = l_4 - c_4,\ \ \bar{x}_5 = l_5 - c_5$$

$$c_1 = \frac{{l_1}^*}{3},\ \ c_2 = \frac{2l_1 + l_2}{3\left(l_1 + l_2\right)}{l_2}^*,\ \ c_3 = \frac{2l_2 + l_3}{3\left(l_2 + l_3\right)}{l_3}^*,$$

$$c_4 = \frac{2l_3 + l_4}{3\left(l_3 + l_4\right)}{l_4}^*,\ \ c_5 = \frac{2l_4 + l_5}{3\left(l_4 + l_5\right)}{l_4}^*$$

$$A_{m1} = \frac{1}{2}{l_1}^*\left(\mathrm{F}l_1\right), A_{m2} = \frac{1}{2}{l_2}^*\left(\mathrm{F}l_1 + \mathrm{F}l_2\right),$$

$$A_{m3} = \frac{1}{2}{l_3}^*\left(\mathrm{F}l_2 + \mathrm{F}l_3\right),\ \ A_{m4} = \frac{1}{2}{l_4}^*\left(\mathrm{F}l_3 + \mathrm{F}l_4\right),$$

$$A_{m5} = \frac{1}{2}{l_5}^*\left(\mathrm{F}l_4 + \mathrm{F}l_5\right)$$

$$I_1 = \frac{1}{64}\pi\left({r_{o1}}^4 - {r_{i1}}^4\right),\ I_2 = 2 \times \frac{1}{12}\left(b_2{h_2}^3\right),$$

$$I_3 = 2 \times \frac{1}{12}\left(b_3{h_3}^3\right),\ I_{31} = 2 \times \frac{1}{12}\left(b_{31}{h_3}^3\right)$$

$$I_4 = \frac{1}{64}\pi\left({r_{o4}}^4 - {r_{i4}}^4\right),$$

$$I_5 = \frac{1}{64}\pi\left({r_{o5}}^4 - {r_{i5}}^4\right)$$

$r_{o1} = 26.4$ mm, $r_{i1} = 25.1$ mm
$b_2 = 3$ mm, $h_2 = 8$ mm
$b_3 = 3$ mm, $h_3 = 1.8$ mm (Latch, dependent here)
$r_{o4} = 26.4$ mm, $r_{i4} = 18.5$ mm
$r_{o5} = 26.4$ mm, $r_{i5} = 25$ mm
$l_1 = 11.5$ mm, $l_2 = 25$ mm, $l_3 = 27$ mm,
$l_4 = 34.6$ mm, $l_5 = 43.6$ mm
${l_1}^* = 11.5$ mm, ${l_2}^* = 13.5$ mm, ${l_3}^* = 2$ mm,
${l_4}^* = 7.6$ mm, $l_5 = 9$ mm
$F = 20$ N (Applied force)
$E = 1.93 \times 10^{11}\mathrm{N/m}^2$ (Elastic modulus of SUS 304)

## References

[1] D. Canes *et al.*, "Transumbilical single-port surgery: Evolution and current status," *Eur. Urol.*, vol. 54, no. 5, pp. 1020–1030, 2008.

[2] M. G. Neto, A. Ramos, and J. Campos, "Single port laparoscopic access surgery," *Techn. Gastrointestinal Endoscopy*, vol. 11, no. 2, pp. 84–93, 2009.

[3] J. H. Kaouk *et al.*, "A novel robotic system for single-port urologic surgery: First clinical investigation," *Eur. Urol.*, vol. 66, no. 6, pp. 1033–1043, 2014.
[4] M. Hwang *et al.*, "A single port surgical robot system with novel elbow joint mechanism for high force transmission," *Int. J. Med. Robot. Comput. Assisted Surgery*, vol. 13, no. 4, 2017, Paper e1808.
[5] Titanmedicalinc.com (homepage on the Internet). Titan Medical, Inc., 2019. [Online]. Available: https://titanmedicalinc.com/technology/
[6] B. Cheon *et al.*, "A single port laparoscopic surgery robot with high force transmission and a large workspace," *Surgical Endoscopy*, vol. 28, no. 9, pp. 2719–2729, 2014.
[7] J. Ding *et al.*, "Design and coordination kinematics of an insertable robotic effectors platform for single-port access surgery," *IEEE/ASME Trans. Mechatronics*, vol. 18, no. 5, pp. 1612–1624, Oct. 2013.
[8] M. Piccigallo *et al.*, "Design of a novel bimanual robotic system for single-port laparoscopy," *IEEE/ASME Trans. Mechatronics*, vol. 15, no. 6, pp. 871–878, Oct. 2010.
[9] SN Shaikh and C. C. Thompson, "Natural orifice translumenal surgery: Flexible platform review," *World J. Gastrointestinal Surgery*, vol. 2, no. 6, pp. 210–216, 2010.
[10] L. Blanc, A. Delchambre, and P. Lambert., "Flexible medical devices: Review of controllable stiffness solutions," *Actuators*, Multidisciplinary Digital Publishing Institute, vol. 6, no. 3, 2017.
[11] V. Saadat, R. C. Ewers, and E. G. Chen, "Shape lockable apparatus and method for advancing an instrument through unsupported anatomy," U.S. Patent No 6,790,173, 2004
[12] Y.-J. Kim *et al.*, "A novel layer jamming mechanism with tunable stiffness capability for minimally invasive surgery," *IEEE Trans. Robot.*, vol. 29, no. 4, pp. 1031–1042, Aug. 2013.
[13] T. Yanagida, K. Adachi, and T. Nakamura, "Development of endoscopic device to veer out a latex tube with jamming by granular materials," in *Proc. IEEE Int. Conf. Robot. Biomimetics*, 2013. pp. 1474–1479.
[14] S. Zuo *et al.*, "Variable stiffness outer sheath with "Dragon skin" structure and negative pneumatic shape-locking mechanism," *Int. J. Comput. Assisted Radiol. Surgery*, vol. 9, no. 5, pp. 857–865, 2014.
[15] R. Zhao, Y. Yao, and Y. Luo, "Development of a variable stiffness over tube based on low-melting-point-alloy for endoscopic surgery," *J. Med. Devices*, vol. 10, no. 2, 2016, Art. no. 021002.
[16] J. Wang *et al.*, "Development of a novel robotic platform with controllable stiffness manipulation arms for laparoendoscopic single-site surgery (LESS)," *Int. J. Med. Robot. Comput. Assisted Surgery*, vol. 14, no. 1, 2018, Paper e1838.
[17] S. Murata *et al.*, "M-TRAN: Self-reconfigurable modular robotic system," *IEEE/ASME Trans. Mechatronics*, vol. 7, no. 4, pp. 431–441, Dec. 2002.
[18] K. Mitsui, R. Ozawa, and T. Kou, "An under-actuated robotic hand for multiple grasps," in *Proc. IEEE/RSJ Int. Conf. Intell. Robot. Syst.*, 2013. pp. 5475–5480.
[19] M. Plooij *et al.*, "Lock your robot: A review of locking devices in robotics," *IEEE Robot. Autom. Mag.*, vol. 22, no. 1, pp. 106–117, Mar. 2015.
[20] D. Molina and V. J. M. Dimaio, "Normal organ weights in men: Part II—the brain, lungs, liver, spleen, and kidneys," *Amer. J. Forensic Med. Pathol.*, vol. 33, no. 4, pp. 368–372, 2012.
[21] R. C. Hibbeler and T. Kiang, *Structural Analysis*. Englewood Cliffs, NJ, USA: Prentice-Hall, 1984, pp. 316–325.
[22] J. A. Wehrmeyer *et al.*, "Colonoscope flexural rigidity measurement," *Med. Biol. Eng. Comput.*, vol. 36, no. 4, pp. 475–479, 1998.
[23] IEC, TS, "60479-1. Effects of current on human beings and livestock–Part 1: General aspects," International Electrotechnical Commission, Geneva, 2005.